

A Rotating Protostellar Jet Launched from the Innermost Disk of HH 212

Chin-Fei Lee^{1,2*}, Paul. T.P Ho^{1,3}, Zhi-Yun Li⁴, Naomi Hirano¹, Qizhou Zhang³, & Hsien Shang¹

¹*Academia Sinica Institute of Astronomy and Astrophysics, P.O. Box 23-141, Taipei 106, Taiwan*

²*Graduate Institute of Astronomy and Astrophysics, National Taiwan University, No. 1, Sec. 4, Roosevelt Road, Taipei 10617, Taiwan*

³*Harvard-Smithsonian Center for Astrophysics, 60 Garden Street, Cambridge, MA 02138*

⁴*Astronomy Department, University of Virginia, Charlottesville, VA 22904*

The central problem in forming a star is the angular momentum in the circumstellar disk which prevents material from falling into the central stellar core. An attractive solution to the “angular momentum problem” appears to be the ubiquitous (low-velocity and poorly-collimated) molecular outflows and (high-velocity and highly-collimated) protostellar jets accompanying the earliest phase of star formation that remove angular momentum at a range of disk radii¹. Previous observations suggested that outflowing material carries away the excess angular momentum via magneto-centrifugally driven winds from the surfaces of circumstellar disks down to ~ 10 AU scales^{2–6}, allowing the material in the outer disk to transport to the inner disk. Here we show that highly collimated protostellar jets remove the residual angular momenta at the ~ 0.05 AU scale, enabling the material in the innermost region of the disk to accrete toward the central protostar. This is supported by the rotation of the jet measured down to ~ 10 AU from the protostar in the HH 212 protostellar sys-

tem. The measurement implies a jet launching radius of $\sim 0.05_{-0.02}^{+0.05}$ AU on the disk, based on the magneto-centrifugal theory of jet production, which connects the properties of the jet measured at large distances to those at its base through energy and angular momentum conservation⁷.

Molecular outflows and protostellar jets together may solve the angular momentum problem in disk accretion. Molecular outflows have been found to trace low-velocity ($\lesssim 20 \text{ km s}^{-1}$) extended winds coming out of the disks down to $\sim 10 \text{ AU}$ scales^{2–6}. They are found to be rotating and thus can remove angular momentum from the disks in the outer part, allowing the disk material in the wind-launching region to accrete. Protostellar jets are much more collimated and denser with a much higher velocity ($\gtrsim 100 \text{ km s}^{-1}$) than the molecular outflows. They are ejected out along the rotational axis from the innermost part of the disks at less than 1 AU scale, and thus are expected to carry away angular momentum from there, allowing the disk material to fall onto the central protostars from the disk truncation radii¹. Tentative measurements of jet rotation have been reported for jets in different evolutionary phases from Class 0 to T-Tauri^{8–17} phase. However, these measurements are quite uncertain because the structures and kinematics across the jet are not well resolved. For example, the rotation of the T Tauri jet in DG Tau measured at $\sim 14 \text{ AU}$ spatial resolution and $\sim 26 \text{ km s}^{-1}$ velocity resolution¹⁴ was later called into question¹⁶ through near-IR integral field observations. Here we report a new measurement of jet rotation in the textbook-case protostellar jet HH 212. Our observations with Atacama Large Millimeter/submillimeter Array (ALMA) have a unique combination of high spatial ($\sim 8 \text{ AU}$ or $0''.02$) and high velocity ($\sim 1 \text{ km s}^{-1}$) resolution, allowing us to measure the smallest specific angular momentum in any jet to date down to 10 AU km s^{-1} scale, as compared to $\sim 30 \text{ AU km s}^{-1}$ scale in previous measurements⁹. We show that jets can indeed remove angular momentum from the innermost disk, enabling material there to accrete toward the central protostar.

HH 212 is a nearby protostellar system deeply embedded in a compact molecular cloud core

in the L1630 cloud of Orion at a distance of ~ 400 pc. The central source is the Class 0 protostar IRAS 05413-0104, with an estimated age of $\sim 40,000$ yrs¹⁸. It has an accretion disk¹⁹ and drives a powerful bipolar jet²⁰. The jet, lying close ($\sim 4^\circ$) to the plane of the sky²¹, is one of the best candidates to search for jet rotation. The systemic velocity is $\sim 1.7 \pm 1.0$ km s⁻¹ LSR in this system¹⁸.

Figure 1a shows our ALMA map of the inner part of the jet within ~ 1200 AU ($3''$) of the central source in SiO J=8-7 at ~ 24 AU ($0''.06$) resolution, together with the dust continuum map (orange image) of the accretion disk at 352 GHz¹⁹. SiO J=8-7 is a dense gas tracer with a critical density of $\sim 10^8$ cm⁻³ and thus traces the jet well. This part of the jet is connected to knots and bow structures NK, SK 1-5 seen on larger scales further out²². In this map, knots SN and SS were detected before but not resolved, and their tips were used to obtain an upper limit of jet rotation⁹. They are now resolved. Knot SN appears as a chain of smaller knots and bow structures along the jet axis, as seen at high-blueshifted velocity in Figure 1b. Here bow structures refer to the ones with bow wings curving backward. These knots and bow structures can be produced by a chain of internal shocks formed by a semi-periodical variation in jet velocity²³. Knot SS appears as an elongated bow structure, as seen at low velocity in Figure 1c, possibly also with a chain of smaller bow structures along the jet axis (see also Figure 1d). Thus, the tips of the SN and SS knots appear to be substantially affected by shock interaction, which makes their previous jet rotation measurements unreliable.

Zooming closer in to the central region, a new chain of knots (N1 to N4 and S1 to S3) are

detected within ~ 120 AU of the central source down to ~ 10 AU, tracing the primary jet emanating from it (see Figure 2a at ~ 8 AU ($0''.02$) resolution). Unfortunately, the disk is flared and optically thick¹⁹, preventing us from detecting the jet further in. The jet is highly collimated with a position angle measured to be $\sim 23^\circ$, exactly perpendicular to the disk major axis. The knots are extremely narrow, with the width (Gaussian deconvolved width, see Methods) decreasing toward the central source, from ~ 9 -16 AU for knots N3 and S3 to $\lesssim 5$ -6 AU for knots N1 and S1 (see Figure 3). Similar decrease in jet width has also been seen in more evolved objects in RW Aur and DG Tau²⁴. These widths are roughly consistent with the width of the H₂O maser measured at ~ 50 AU about 20 yrs ago²¹. For the knots further out, SS and SN, the width has been previously estimated to be ~ 80 AU at 400-800 AU in SiO J=5-4²⁵.

Except for knot N4 that shows a bow wing on the east side of the jet axis, the new knots do not show any hint of bow structures, allowing us to measure radial velocity gradients with more confidence. These knots are closest to the central source, and thus expected to be least affected by shocks²³. Figure 4 shows the position-velocity (PV) diagrams of the SiO emission cut across the knots (see Figure 2 for the cuts). Knots N1, S1, and S2 are not resolved, and thus no velocity gradient can be detected. Note that for knots S1 and N3, SiO emissions (marked with a “?”) at (~ 5 km s⁻¹ LSR, ~ 4 -12 AU) and (~ -3 km s⁻¹ LSR, ~ -4 to -12 AU), respectively, are offset from the rest of the SiO emission and are thus likely not from the jet itself. Knots N2, N3, and S3 are marginally resolved. A velocity gradient can be seen across them at more than 7σ detection (as marked by the red contours) around the mean jet velocity (vertical dashed line). With respect to the mean jet velocity, the blueshifted emission is seen mostly on the west side of the

knot and the redshifted emission mostly on the east. To measure the gradient, we identified the emission peaks (as marked by the green squares) with Gaussian fits and then fitted them with a linear velocity gradient using the least squares method. As marked by the solid lines, the gradients are 0.363 ± 0.040 AU/(km s⁻¹) for knot N2 over the velocity range from -7.5 to 2.6 km s⁻¹, 0.533 ± 0.326 AU/(km s⁻¹) for knot N3 over the velocity range from -7.5 to 1.0 km s⁻¹, and 0.635 ± 0.070 AU/(km s⁻¹) for knot S3 over the velocity range from 0.12 to 8.6 km s⁻¹. Since the sense of the gradient is the same in the resolved knots, the gradients are unlikely due to random velocity fluctuations in the jet. The gradients are also unlikely due to jet precession, which was found to be small with an opening angle of $\sim 1^\circ$ and a period of ~ 100 yrs²². The consistency of the sense of the gradients supports the interpretation that they are dominated by the intrinsic jet rotation. Moreover, this sense of velocity gradient is the same as that for the rotation of the disk^{18,26}, further supporting such an interpretation. Note that the rotation sense of the disk is confirmed in our new ALMA observations of the disk in deuterated methanol at ~ 16 AU resolution down to the center²⁷. The velocity gradient can be seen more pictorially in Figure 2b, where the redshifted and blueshifted emissions are plotted separately for each knot. For those resolved knots, N2, N3, and S3, the redshifted emission is seen mostly on the east and the blueshifted emission mostly on the west of the jet axis. The same split of emission can also be seen in the unresolved knot, N1. This spatial distribution of the redshifted and blueshifted emission indicates that both the northern and southern jets are rotating clockwise when viewed along the jet axis from north to south, in the same direction as the disk rotation (marked by curved arrows in Figure 2b). Assuming that the jet rotation is symmetric about the knot center, then the resulting specific angular momentum

is $l = m(\Delta V)^2/4$, where m is the gradient derived above and ΔV is the velocity range used to derive the gradient. Thus, the specific angular momentum is estimated to be $\sim 9.4 \pm 1.0$, 9.6 ± 6.0 , and 11.4 ± 1.3 AU km s⁻¹ for knots N2, N3, and S3, respectively. Excluding the value of knot N3, which is quite uncertain, the mean specific angular momentum is $l_j \sim 10.2 \pm 1.0$ AU km s⁻¹.

Protostellar jets are generally thought to be launched magneto-centrifugally from disks¹. In particular, two competing models, the X-wind model²⁸ and disk-wind model²⁹, have been constructed for jet launching from the accretion disks through the magneto-centrifugal mechanism. In this framework, the launching radius of the jet can be derived from the specific angular momentum and the velocity of the jet, based on conservation of energy and angular momentum, if the mass of the central protostar is known⁷ (see also Methods). With a protostellar mass of $M_* \sim 0.25 \pm 0.05 M_\odot$ ^{18,26}, a jet velocity²² of $v_j \sim 115 \pm 50$ km s⁻¹, and a mean jet specific angular momentum of $l_j \sim 10.2 \pm 1.0$ AU km s⁻¹, the launching radius of the jet is estimated to be $r_0 \sim 0.05^{+0.05}_{-0.02}$ AU, using Eq. 2 in Methods.

Since HH 212 has a bolometric luminosity $\sim 9 L_\odot$, the dust sublimation radius should be larger than 0.1 AU³⁰, which is outside our inferred jet launching radius. An implication is that Si is already released from the grains into the gas phase at the base of the jet. However, since the jet is well collimated with a high mass-loss rate²² of $\sim 10^{-6} M_\odot$ yr⁻¹, SiO is expected to form rather quickly because of the high density in the jet³¹. In addition, the Si⁺ recombination and SiO formation are expected to be faster than the photodissociation caused by possible far-ultraviolet radiation of the central protostar³².

Since the SiO jet extracts the angular momentum from the innermost region of the disk, the angular momentum problem is only partially resolved because material still has to be transported within the disk to its innermost region¹. This transfer within the disk may be achieved with other mechanisms, e.g., magneto-rotational instability³³ and low-velocity extended tenuous disk wind²⁹. Recent ALMA CH₃OH observations at ~ 240 AU resolution have suggested a disk wind component in HH 212 ejected from the disk at a radius of ~ 1 AU³⁴, surrounding the SiO jet. However, our new observations at ~ 16 AU resolution show that CH₃OH actually traces the disk surface within ~ 40 AU of the center²⁷. Disk wind has also been suggested in other objects, e.g., CB 26³, DG Tau²⁴, Orion BN/KL Source I^{2,4,5}, and TMC1A⁶. For example, in Orion BN/KL Source I, a low-velocity and poorly-collimated bipolar outflow was found in SiO maser to come from the disk surface at larger disk radii of $\gtrsim 20$ AU from the central source^{2,4,5}. Similarly in TMC1A, a low-velocity and poorly-collimated CO outflow was found to come from the disk surface at larger disk radii of up to 25 AU from the central source⁶. All these suggest the presence of a disk wind component extracting the angular momentum from the disk at larger radii. In contrast, the SiO jet in HH 212 appears to come from the innermost region of the disk, well inside 1 AU of the central star. It is consistent with the X-wind picture²⁸, but could also be the innermost part of a more extended disk-wind²⁹.

Our observations have a unique combination of high spatial and velocity resolution, allowing us to measure radial velocity gradients and hence estimate the smallest specific angular momentum in any jet to date. The measured small specific angular momentum implies a fast jet launched from the innermost region of the disk for the first time in the earliest phase of star formation.

Our measurement sets the tightest constraint yet on the location of protostellar jet launching. It also opens up an exciting opportunity to study jet rotation and launching location in other young systems.

Methods

Observations Observations of the HH 212 protostellar system were carried out with ALMA in Band 7 at ~ 350 GHz in Cycles 1 and 3, with 32-45 antennas (see Supplementary Table 1). The Cycle 1 project was carried out with 2 executions, both on 2015 August 29 during the Early Science Cycle 1 phase. The projected baselines are 15-1466 m. The maximum recoverable size scale is $\sim 2''.5$. A 5-pointing mosaic was used to map the jet within $\sim 15''$ of the central source at an angular resolution of $\sim 0''.16$ (64 AU). The Cycle 3 project was carried out with 2 executions in 2015, one on November 5 and the other on December 3, during the Early Science Cycle 3 phase. The projected baselines are 17-16196 m. The maximum recoverable size scale is $\sim 0''.4$. One pointing was used to map the innermost part of the jet at an angular resolution of $0''.02$ (8 AU). For the Cycle 1 project, the correlator was set up to have 4 spectral windows, with one for CO $J = 3 - 2$ at 345.795991 GHz, one for SiO $J = 8 - 7$ at 347.330631 GHz, one for HCO⁺ $J = 4 - 3$ at 356.734288 GHz, and one for the continuum at 358 GHz (see Supplementary Table 2). For the Cycle 3 project, the correlator was more flexible and thus was set up to include 2 more spectral windows, with one for SO $N_J = 8_9 - 7_8$ at 346.528481 GHz and one for H¹³CO⁺ $J = 4 - 3$ at 346.998338 GHz (see Supplementary Table 3). The total time on the HH 212 system is ~ 148 minutes.

In this paper, we only present the observational results in SiO, which traces the jet emanating from the central source. The velocity resolution is 0.212 km s^{-1} per channel. However, we binned 4 channels to have a velocity resolution of 0.848 km s^{-1} in order to map the jet with sufficient sensitivities. The data were calibrated with the CASA package (versions 4.3.1 and 4.5) for

the passband, flux, and gain (see Supplementary Table 4). We used a robust factor of 2 (natural weighting) for the visibility weighting to generate the SiO maps. In order to avoid the proper motion effect (~ 2 AU or $0''.005$ per month using 115 km s^{-1} for the jet velocity²²), only Cycle 3 data are used to study the jet rotation in the innermost part of the jet. This generates a synthesized beam with a size of $0''.02$ (8 AU) for the maps of the innermost part of the jet (see Figure 2). In order to map the knots further out, which are more extended, we also include the Cycle 1 data, which has a larger maximum recoverable scale. In addition, a taper of $0''.05$ was used to degrade the beam size to $0''.06$ (24 AU, see Figure 1) in order to improve the S/N ratio. The noise levels can be measured from line-free channels and are found to be $\sim 1.6 \text{ mJy beam}^{-1}$ (or $\sim 40 \text{ K}$) for a beam of $\sim 0''.02$ (8 AU) and $1.9 \text{ mJy beam}^{-1}$ (or $\sim 6 \text{ K}$) for a beam of $\sim 0''.06$ (24 AU), respectively. The velocities in the channel maps and the resulting position-velocity diagrams are LSR.

Gaussian deconvolved width of the jet knots: Supplementary Figure 1 shows the spatial profile of the jet knots perpendicular to the jet axis, extracted from the SiO total intensity map shown in Figure 2a (see the white lines for the cuts). In order to derive the width of the knots, we fitted the spatial profiles of the knots with a gaussian profile. For knot S1, the emission at $\sim 4\text{-}12$ AU is unlikely from the jet itself, as discussed in the main text, and is thus excluded from the fitting. The deconvolved width is the width deconvolved with the beam size of ~ 8 AU ($0''.02$). Knots N2, N3, and S3 have a deconvolved width greater than the beam size. Knots N1, S1, and S2 have a deconvolved width smaller than the beam size.

Mean (or Systemic) Velocities of the Jet: Supplementary Figure 2 shows the position-velocity diagram of the SiO jet cut along the jet axis. The northern jet component is detected from ~ -14

to 8 km s^{-1} LSR, with a mean velocity of $\sim -3 \text{ km s}^{-1}$ LSR (as indicated by the vertical dashed line). The southern jet component is detected from ~ -5 to 13 km s^{-1} LSR, with a mean velocity of $\sim 4 \text{ km s}^{-1}$ LSR (as indicated by the vertical dashed line). These mean velocities are taken to be the systemic velocities in the northern and southern jet components.

Estimation of Jet Launching Radius Protostellar jets are generally thought to be launched magnetocentrifugally from disks¹. In this framework, the launching radius of the jet can be derived from the specific angular momentum and the velocity of the jet, based on conservation of energy and angular momentum along the field line, if the mass of the central protostar is known⁷. For HH 212, since (1) the jet velocity (poloidal velocity) is so high that the gravitational potential can be neglected at large distances, (2) the jet velocity is much higher than the jet rotation, and (3) the jet inclination angle is very small ($\sim 4^\circ$)²¹, the governing equation (Eq. 4 in Anderson et al. 2003)⁷ that is used to derive the jet launching radius can be simplified and rewritten as

$$\frac{2l_j}{v_j^2} \left(\frac{GM_*}{r_0} \right)^{1/2} - \frac{3GM_*}{v_j^2} - r_0 \approx 0 \quad (1)$$

in order to find approximate solutions analytically, where r_0 is the launching radius at the footpoint, v_j is the jet velocity, l_j is the specific angular momentum of the jet measured at a large distance, and M_* is the mass of the central protostar. Solving this equation, we find the jet launching radius to be

$$r_0 \approx \left(\frac{2l_j}{v_j^2} \right)^{2/3} (GM_*)^{1/3} \left[1 - \frac{2}{3}\eta + \frac{1}{9}\eta^2 \right] \quad (2)$$

with

$$\eta = \frac{3}{2^{2/3}} \left(\frac{GM_*}{v_j l_j} \right)^{2/3} \quad (3)$$

Note that the second and third terms are the correction terms to the previous solution (Eq. 5 in Anderson et al. 2003)⁷. They can improve the accuracy of the launching radius estimate in the case where the dimensionless parameter η is not much smaller than unity, particularly when the specific angular momentum l is relatively small, as is true for HH212.

1. Frank, A., and 12 colleagues, Jets and Outflows from Star to Cloud: Observations Confront Theory. *Protostars and Planets VI*, 451-474 (2014).
2. Greenhill, L. J., C. R. Gwinn, C. Schwartz, J. M. Moran, and P. J. Diamond, Coexisting conical bipolar and equatorial outflows from a high-mass protostar. *Nature*, **396**, 650-653 (1998).
3. Launhardt, R., Y. Pavlyuchenkov, F. Gueth, X. Chen, A. Dutrey, S. Guilloteau, T. Henning, V. Piétu, K. Schreyer, and D. Semenov, Rotating molecular outflows: the young T Tauri star in CB 26. *A&A*, **494**, 147-156 (2009).
4. Matthews, L. D., L. J. Greenhill, C. Goddi, C. J. Chandler, E. M. L. Humphreys, and M. W. Kunz, A Feature Movie of SiO Emission 20-100 AU from the Massive Young Stellar Object Orion Source I. *ApJ*, **708**, 80-92 (2010).
5. Greenhill, L. J., C. Goddi, C. J. Chandler, L. D. Matthews, and E. M. L. Humphreys, Dynamical Evidence for a Magnetocentrifugal Wind from a $20 M_{\odot}$ Binary Young Stellar Object. *ApJL*, **770**, L32 (2013).
6. Bjerkeli, P., M. H. D. van der Wiel, D. Harsono, J. P. Ramsey, and J. K. Jørgensen, Resolved images of a protostellar outflow driven by an extended disk wind. *Nature*, **540**, 406-409 (2016).
7. Anderson, J. M., Z.-Y. Li, R. Krasnopolsky, and R. D. Blandford, Locating the Launching Region of T Tauri Winds: The Case of DG Tauri. *ApJL*, **590**, L107-L110 (2003).
8. Codella, C., S. Cabrit, F. Gueth, R. Cesaroni, F. Bacciotti, B. Lefloch, and M. J. McCaughrean, A highly-collimated SiO jet in the HH212 protostellar outflow. *A&A*, **462**, L53-L56 (2007).

9. Lee, C.-F., P. T. P. Ho, T. L. Bourke, N. Hirano, H. Shang, and Q. Zhang, SiO Shocks of the Protostellar Jet HH 212: A Search for Jet Rotation. *ApJ*, **685**, 1026-1032 (2008).
10. Lee, C.-F., N. Hirano, A. Palau, P. T. P. Ho, T. L. Bourke, Q. Zhang, and H. Shang, Rotation and Outflow Motions in the Very Low-Mass Class 0 Protostellar System HH 211 at Subarcsecond Resolution. *ApJ*, **699**, 1584-1594 (2009).
11. Zapata, L. A., J. Schmid-Burgk, D. Muders, P. Schilke, K. Menten, and R. Guesten, A rotating molecular jet in Orion. *A&A*, **510**, A2(2010).
12. Chen, X., H. G. Arce, Q. Zhang, R. Launhardt, and T. Henning, Rotating Bullets from A Variable Protostar. *ApJ*, **824**, 72 (2016).
13. Chrysostomou, A., F. Bacciotti, B. Nisini, T. P. Ray, J. Eislöffel, C. J. Davis, and M. Takami, Investigating the transport of angular momentum from young stellar objects. Do H2 jets from class I YSOs rotate?. *A&A*, **482**, 575-583 (2008).
14. Bacciotti, F., T. P. Ray, R. Mundt, J. Eislöffel, and J. Solf, Hubble Space Telescope/STIS Spectroscopy of the Optical Outflow from DG Tauri: Indications for Rotation in the Initial Jet Channel. *ApJ*, **576**, 222-231 (2002).
15. Coffey, D., F. Bacciotti, T. P. Ray, J. Eislöffel, and J. Woitas, Further Indications of Jet Rotation in New Ultraviolet and Optical Hubble Space Telescope STIS Spectra. *ApJ*, **663**, 350-364 (2007).
16. White, M. C., McGregor, P. J., Bicknell, G. V., et al. 2014, *MNRAS*, 441, 1681

17. Coffey, D., C. Dougados, S. Cabrit, J. Pety, and F. Bacciotti, A Search for Consistent Jet and Disk Rotation Signatures in RY Tau. *ApJ*, **804**, 2 (2015).
18. Lee, C.-F., N. Hirano, Q. Zhang, H. Shang, P. T. P. Ho, and R. Krasnopolsky, ALMA Results of the Pseudodisk, Rotating Disk, and Jet in the Continuum and HCO^+ in the Protostellar System HH 212. *ApJ*, **786**, 114 (2014).
19. Lee, C.-F., Li, Z-Y, Ho, P. T. P., Hirano, N., Zhang, Q., and Shang, H., First detection of equatorial dark dust lane in a protostellar disk at submillimeter wavelength. *Sci. Ad.*, **3** e1602935 (2017)
20. Zinnecker, H., M. J. McCaughrean, and J. T. Rayner, A symmetrically pulsed jet of gas from an invisible protostar in Orion. *Nature*, **394**, 862-865 (1998).
21. Claussen, M. J., K. B. Marvel, A. Wootten, and B. A. Wilking, Distribution and Motion of the Water Masers near IRAS 05413-0104. *ApJL*, **507**, L79-L82 (1998).
22. Lee, C.-F., N. Hirano, Q. Zhang, H. Shang, P. T. P. Ho, and Y. Mizuno, Jet Motion, Internal Working Surfaces, and Nested Shells in the Protostellar System HH 212. *ApJ*, **805**, 186 (2015).
23. Moraghan, A., C.-F. Lee, P.-S. Huang, and B. Vaidya, A study of the wiggle morphology of HH 211 through numerical simulations. *MNRAS*, **460**, 1829-1838 (2016).
24. Agra-Amboage, V., C. Dougados, S. Cabrit, and J. Reunanen, Sub-arcsecond [Fe ii] spectro-imaging of the DG Tauri jet. Periodic bubbles and a dusty disk wind?. *A&A*, **532**, A59 (2011).

25. Cabrit, S., C. Codella, F. Gueth, B. Nisini, A. Gusdorf, C. Dougados, and F. Bacciotti, PdBI sub-arcsecond study of the SiO microjet in HH212. Origin and collimation of class 0 jets. *A&A*, **468**, L29-L32 (2007).
26. Codella, C., and 10 colleagues, The ALMA view of the protostellar system HH212. The wind, the cavity, and the disk. *A&A*, **568**, L5 (2014).
27. Lee, C.-F., Li, Z.-Y., Ho, P. T. P., Hirano, N., Zhang, Q., and Shang, H., Formation and Atmosphere of Complex Organic Molecules of the HH 212 Protostellar Disk. *ApJ*, **Submitted**.
28. Shu, F. H., J. R. Najita, H. Shang, and Z.-Y. Li, X-Winds Theory and Observations. *Protostars and Planets*, **IV**, 789-814 (2000).
29. Konigl, A. and R. E. Pudritz, Disk Winds and the Accretion-Outflow Connection. *Protostars and Planets*, **IV**, 759 (2000).
30. Millan-Gabet, R., F. Malbet, R. Akeson, C. Leinert, J. Monnier, and R. Waters, The Circumstellar Environments of Young Stars at AU Scales. *Protostars and Planets*, **V**, 539-554 (2007).
31. Glassgold, A. E., G. A. Mamon, and P. J. Huggins, The formation of molecules in protostellar winds. *ApJ*, **373**, 254-265 (1991).
32. Cabrit, S., C. Codella, F. Gueth, and A. Gusdorf, High SiO abundance in the HH212 protostellar jet. *A&A*, **548**, L2 (2012).
33. Balbus, S. A. and J. F. Hawley, An Exact, Three-dimensional, Time-dependent Wave Solution in Local Keplerian Flow. *ApJ*, **652**, 1020-1027 (2006).

34. Leurini, S., and 11 colleagues, Hot methanol from the inner region of the HH 212 protostellar system. *A&A*, **595**, L4 (2016).

Correspondence and Requests for Materials should be addressed to Chin-Fei Lee.

Acknowledgements This paper makes use of the following ALMA data: ADS/JAO.ALMA#2012.1.00122.S and 2015.1.00024.S. ALMA is a partnership of ESO (representing its member states), NSF (USA) and NINS (Japan), together with NRC (Canada), NSC and ASIAA (Taiwan), and KASI (Republic of Korea), in co-operation with the Republic of Chile. The Joint ALMA Observatory is operated by ESO, AUI/NRAO and NAOJ. C.-F.L. acknowledges grants from the Ministry of Science and Technology of Taiwan (MoST 104-2119-M-001-015-MY3) and the Academia Sinica (Career Development Award). ZYL is supported in part by NASA NNX14AB38G and NSF AST 1313083.

Author Contributions C.-F. Lee led the project, analysis, discussion, and drafted the manuscript. P.T.P. Ho and Z.-Y. Li commented on the manuscript and participated in the discussion. All other coauthors contribute to scientific discussion.

Data Availability Statement This letter makes use of the following ALMA data: ADS/JAO.ALMA#2012.1.00122.S and 2015.1.00024.S. The data that support the plots within this paper and other findings of this study are available from the corresponding author upon reasonable request.

Competing interests The authors declare no competing financial interests.

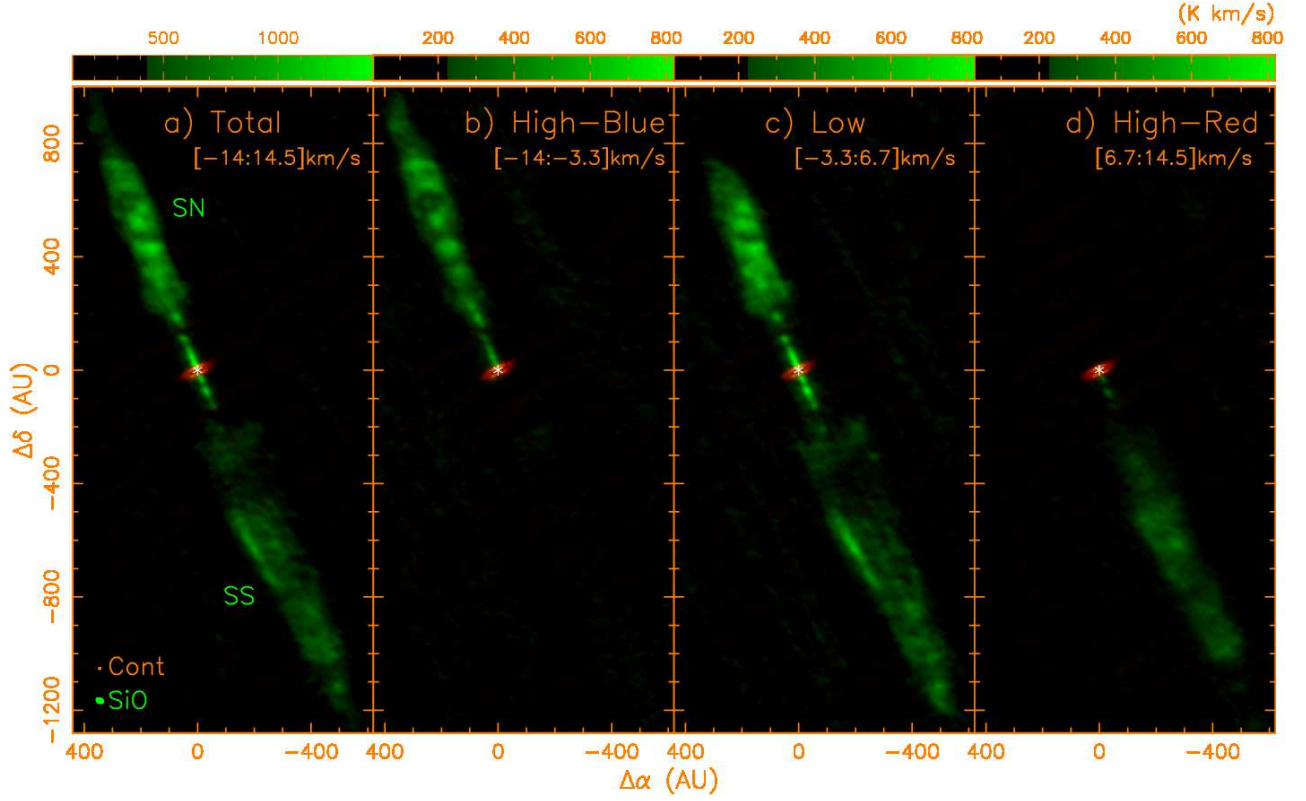


Figure 1. ALMA SiO J=8-7 maps (green images) of the jet at a spatial resolution of ~ 24 AU ($0''.06$), on top of the dust continuum map (orange image) of the accretion disk at 352 GHz¹⁹. The velocity ranges used for the SiO emission are indicated in the brackets in the upper right corner. The systemic velocity is assumed to be 1.7 ± 0.1 km s⁻¹ LSR, as found before¹⁸. Velocities within 5 km s⁻¹ of the systemic velocity are referred to as low and those outside the range as high. Asterisks mark the source position at $\alpha_{(2000)} = 05^{\text{h}}43^{\text{m}}51^{\text{s}}.4086$, $\delta_{(2000)} = -01^{\circ}02'53''.147^{19}$.

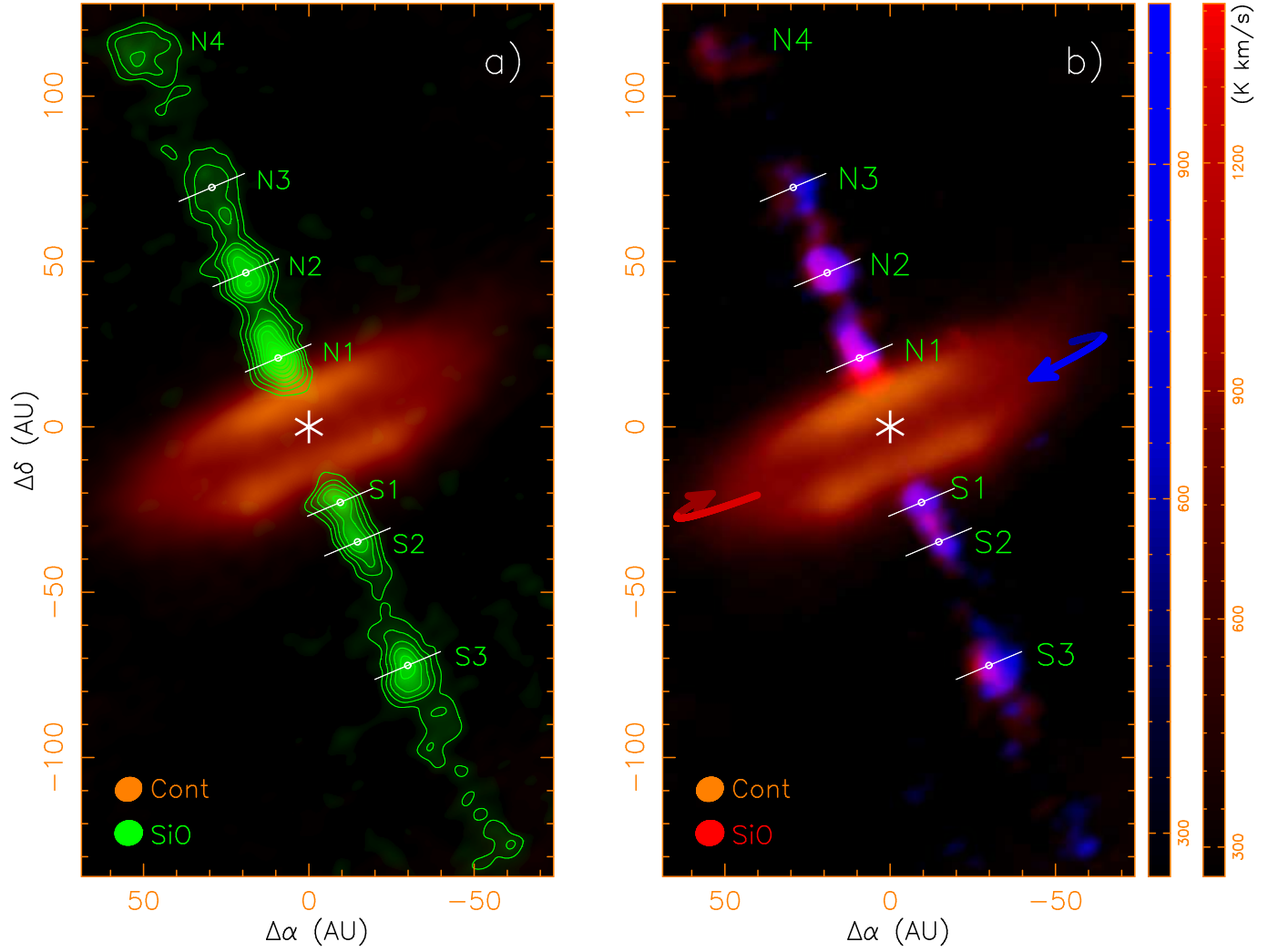


Figure 2. A zoom-in to the innermost part of the jet in SiO within ~ 120 AU ($0''.3$) of the central source, at an angular resolution of ~ 8 AU ($0''.02$), on top of the continuum map of the disk. The maps show the intensity (in unit of K km s^{-1}) integrated over certain velocity range as given in the later part of the caption. White lines mark the cuts used to extract the spatial profiles and the position-velocity diagrams of the knots, with dots being the centers. (a) A chain of new knots (N1..N4, S1..S3) are detected, tracing the primary jet emanating from the disk. The SiO

is integrated from ~ -14 to 14.5 km s^{-1} LSR. Contour levels start from 3σ with a step of 1.5σ , where $\sigma = 330 \text{ K km s}^{-1}$. (b) Blueshifted and redshifted SiO emission of the jet plotted with the continuum emission. In the north, the velocity ranges of the blueshifted and redshifted emission are ~ -10 to -5 km s^{-1} LSR and -1 to 4 km s^{-1} LSR, respectively. In the south, the velocity ranges of the blueshifted and redshifted emission are ~ -3 to 2 km s^{-1} LSR and 6 to 11 km s^{-1} LSR, respectively. The direction of disk rotation is depicted by curved arrows.

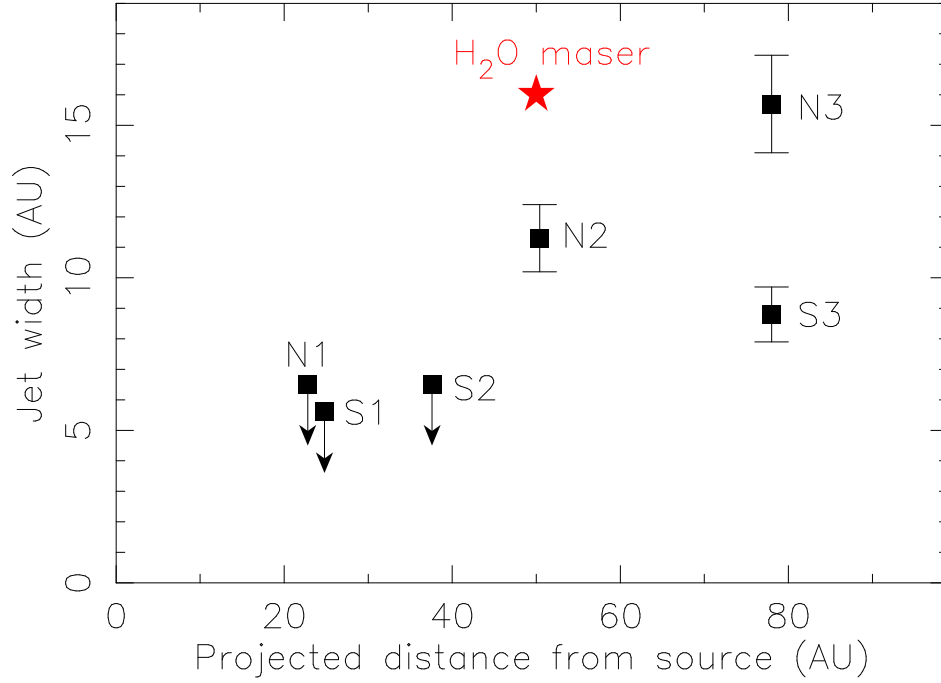


Figure 3. The jet (gaussian deconvolved) width measured for the new knots within ~ 100 AU of the source. The “star” marks the H_2O maser width measured by VLBI about 20 yrs ago²¹. The error bars show the uncertainties in the width. The down arrows indicate that the measured widths are the upper limits.

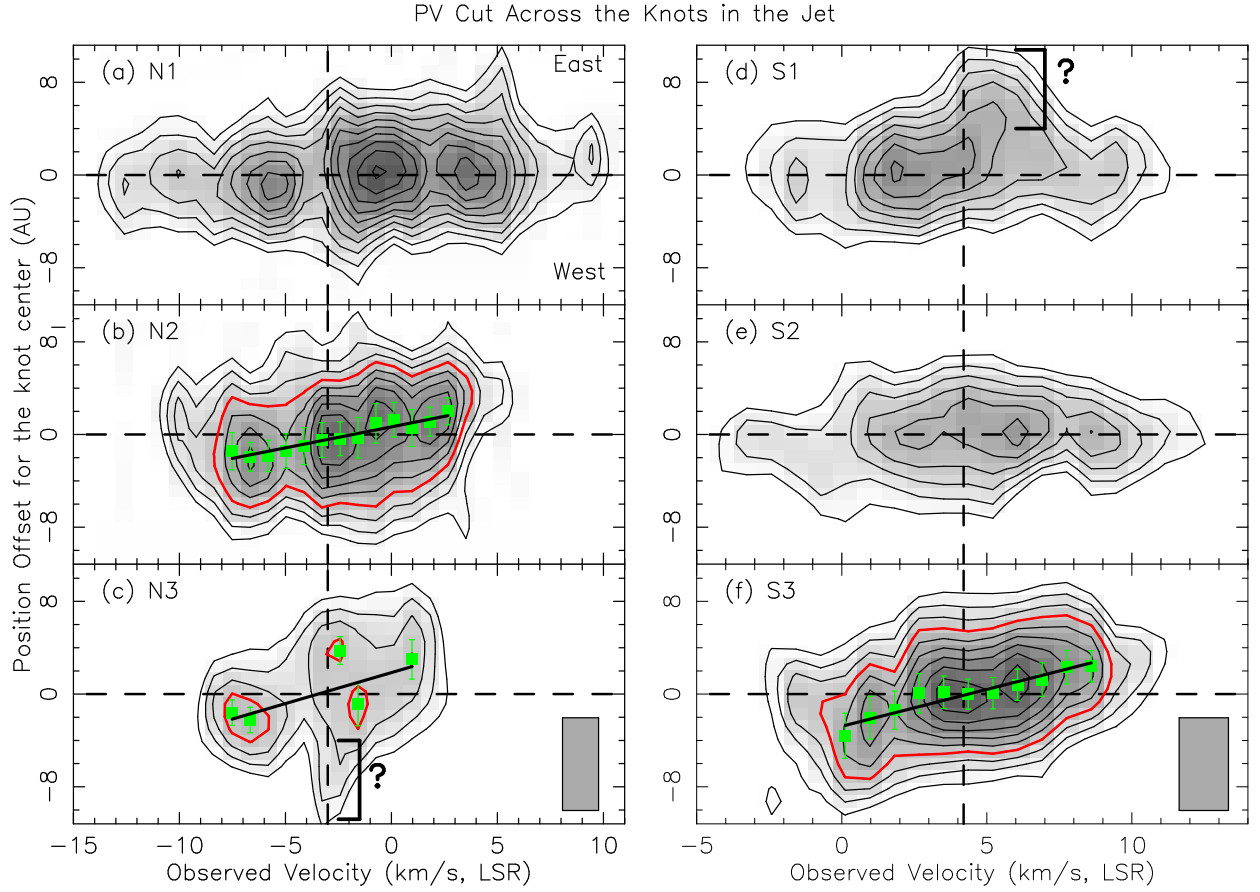


Figure 4. Position-velocity (PV) diagrams cut across the knots (N1..N3 and S1..S3) in the jet. The horizontal dashed lines indicate the peak (central) position of the knots. The vertical dashed lines indicate roughly the systemic (mean) velocities for the northern and southern jet components (as in Figure 2, see Methods). The contour levels start from 4σ with a step of 1σ , where $\sigma = 21.3$ K. The red contours mark the 7σ detections in knots N2, N3, and S3. For knots N3 and S1, the emissions marked with “?” are likely not from the jet itself. The green squares mark the emission peak positions with more than 7σ detections, as determined from the Gaussian fits. The error bars show the uncertainties in the peak positions, which are assumed to be given by a quarter of the FWHM. The solid lines mark the linear velocity structures across the knots. The bars indicate the

angular (8 AU or $\sim 0''.02$) and velocity ($\sim 1.7 \text{ km s}^{-1}$) resolutions used for the PV cuts.